VIRTUAL OBSERVATORY: Plate Content Digitization, Archive Mining & Image Sequence Processing
edited by M. Tsvetkov, V. Golev, F. Murtagh, and R. Molina, Heron Press, Sofia, 2005

Super resolution reconstruction of multispectral images*

R. Molina[1], **J. Mateos**[1], **A. K. Katsaggelos**[2]

[1]Departamento de Ciencias de la Computación e I. A.
Universidad de Granada, 18071 Granada, Spain.

[2]Department of Electrical and Computer Engineering, Northwestern University, Evanston, Illinois 60208-3118.

Abstract.

Multispectral image reconstruction allows to combine a multispectral low resolution image with a panchromatic high resolution one to obtain a new multispectral image with the spectral properties of the lower resolution image and the level of detail of the higher resolution one. In this paper we formulate the problem of multispectral image reconstruction based on super-resolution techniques and derive an iterative method to estimate the high resolution multispectral image from the observed images. Finally, the proposed method is tested on a real Landsat 7 ETM+ image.

1 Introduction

Multispectral images are of interest in commercial, civilian or military areas with a wide range of applications including GPS guidance maps, land type and usage measures or target detection, among others. Nowadays most remote sensing systems include sensors able to capture, simultaneously, several low resolution images of the same area on different wavelengths, forming a multispectral image, along with a high resolution panchromatic image. The main characteristics of such remote sensing systems are the number of bands of the multispectral image and the resolution of those bands and the panchromatic image. For instance, the Landsat 7 satellite (`http://landsat.gsfc.nasa.gov/`), equipped with the ETM+ sensor, allows for the capture of a multispectral image with six bands (three bands on the visible spectrum plus three bands on the infrared) with a resolution of 30 meters per pixel, a thermal band with a resolution of 60 meters

*This work has been supported by the "Comisión Nacional de Ciencia y Tecnología" under contract TIC2003-00880.

per pixel and a panchromatic band (covering a large zone on the visible spectrum and the near infrared), with a resolution of 15 meters per pixel.

The main advantage of the multispectral image is to allow for a better land type and use recognition but, due to its lower resolution, information on the objects shape and texture may be lost. On the other hand, the panchromatic image allows a better recognition of the objects in the image and their textures but gives no information about their spectral properties.

Through this paper we will use the term multispectral image reconstruction to refer to the joint processing of the multispectral and panchromatic images in order to obtain a new multispectral image that, ideally, will present the spectral characteristics of the observed multispectral image and the resolution and quality of the panchromatic image. The use of this technique, also named *pansharpening*, will allow us to obtain, in the case of Landsat 7 ETM+, a multispectral image with a resolution of 15 meters per pixel.

A few approximations to this problem have been proposed in the literature. With the Intensity, Hue, Saturation (IHS) transformation method [2], the multispectral image is transformed from the RGB color space into the IHS domain. Then, the intensity component is replaced by the histogram matched panchromatic image and the hue and saturation components are resampled to the panchromatic resolution. The inverse IHS transformation is performed to return to the RGB domain. In [4] after principal component analysis (PCA) is applied to the multispectral image bands, the first principal component is replaced by the panchromatic image and the inverse PCA transform is computed to go back to the image domain. Some wavelets based approach have been also proposed. In [5], for instance, a redundant wavelets transform is applied to the multispectral and panchromatic images and some of the transformed bands of the multispectral image are either added or substituted by the transform bands of the panchromatic image. A comparison of such techniques can be found in [9]. Price [7] proposed a method relying on image based statistical relationships between the radiances in the low and high spatial resolution bands. Later, Park and Kang [6] modified the statistics estimation method to include spatial adaptativity. Recently a few super-resolution based methods has been proposed. Eismann *et al.* [3] proposed a MAP approach that makes use of a stochastic mixing model of the underlying spectral scene content to achieve resolution enhancement beyond the intensity component of the hyperspectral image. Akgun *et al.* [1] proposed a POCS based algorithm to reconstruct hyperspectral images where the hyperspectral observations from different wavelengths are represented as weighted linear combinations of a small number of basis image planes. In this paper we also formulate the problem of multispectral image reconstruction based on super-resolution techniques and derive an iterative method to estimate the high resolution multispectral image from the observed images.

The paper is organized as follows. The acquisition model is presented in section 2. In section 3 the Bayesian paradigm for multispectral image reconstruction is presented and the required probability distributions are formulated.

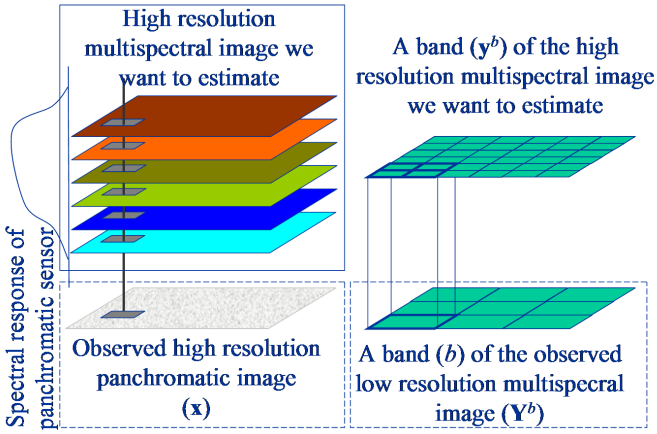

Figure 1. Acquisition model and used notation.

The Bayesian analysis is performed in section 4 to obtain the reconstruction algorithm. Experimental results on a real Landsat 7 ETM+ image are described in section 5 and, finally, section 6 concludes the paper.

2 Acquisition model

Let us assume that the multispectral image we would observe under ideal conditions with a high resolution sensor has B bands, each one of size $p = m \times n$ pixels. Each band of this image can be expressed as a column vector by lexicographically ordering the pixels on the band as

$$\mathbf{y}^b = [y^b(1,1), y^b(1,2), \ldots, y^b(m,n)]^t, \quad b = 1, 2, \ldots, B,$$

where t denotes the transpose of a vector or matrix.

However, in real applications, this image is not available and, instead, we observe a low multispectral resolution image with $P = M \times N$ pixels, $M < m$ and $N < n$, and B bands. Using the previously described ordering, the observed bands can be expressed as column vectors as

$$\mathbf{Y}^b = [Y^b(1,1), Y^b(1,2), \ldots, Y^b(M,N)]^t, \quad b = 1, 2, \ldots, B.$$

Figure 1 illustrates the acquisition model and the used notation.

Each band, $\mathbf{Y}^b$, is related to its corresponding high resolution image by

$$\mathbf{Y}^b = \mathbf{H}^b \mathbf{y}^b + \mathbf{n}^b, \quad \forall b = 1, \cdots, B, \tag{1}$$

where $\mathbf{H}^b$ is a $p \times P$ matrix representing the blurring, the sensor integration function and the spatial subsampling and $\mathbf{n}^b$ is the capture noise, assumed to be Gaussian with zero mean and variance $\beta^{b^{-1}}$.

A simple but widely used model for the matrix $\mathbf{H}^b$ is to consider that each pixel (i,j) of the low resolution image is obtained according to (for $m = 2M$ and $n = 2N$)

$$Y^b(i,j) = \frac{1}{4} \sum_{(u,v)\in E_{i,j}} y^b(u,v) + n^b(i,j), \tag{2}$$

where $E_{i,j}$ consists of the indices of the four high resolution pixels $E_{i,j} = \{(2i,2j),(2i+1,2j),(2i,2j+1),(2i+1,2j+1)\}$ (see right hand side of figure 1).

The sensor also provides us with a panchromatic image $\mathbf{x}$ of size $p = m \times n$, obtained by spectral averaging the high resolution images $\mathbf{y}^b$. This relation can be modelled as

$$\mathbf{x} = \sum_{b=1}^{B} \lambda^b \mathbf{y}^b + \nu, \tag{3}$$

where $\lambda^b \geq 0$, $b = 1, 2, \cdots, B$, are known quantities that can be obtained, as we will see later, from the sensor spectral characteristics, and weight the contribution of each band $\mathbf{y}^b$ to the panchromatic image $\mathbf{x}$ (see left hand side of figure 1), and ν is the capture noise that is assumed to be Gaussian with zero mean and variance γ^{-1}.

3 Bayesian Paradigm

Our aim is to reconstruct a specified multispectral image band, $\mathbf{y}^b$, from its corresponding observed low resolution band $\mathbf{Y}^b$ and the high resolution panchromatic image $\mathbf{x}$. In this paper we also assume that we have estimates of the multispectral high resolution bands $\mathbf{y}^{\overline{b}}$, $\overline{b} = \{j = 1, \ldots, B, j \neq b\}$, that is, the rest of the bands of the high resolution multispectral image.

Bayesian methods start with a prior distribution, a probability distribution over images $\mathbf{y}^b$ where we incorporate information on the expected structure within an image. In the Bayesian framework it is also necessary to specify $p(\mathbf{Y}^b|\mathbf{y}^b, \mathbf{y}^{\overline{b}})$ and $p(\mathbf{x}|\mathbf{y}^b, \mathbf{y}^{\overline{b}})$ the probability distributions of the observed low resolution image bands $\mathbf{Y}^b$ and the panchromatic image $\mathbf{x}$ if $\mathbf{y}^b$ and $\mathbf{y}^{\overline{b}}$ were the 'true' high resolution multispectral image bands. These distributions model how the observed images have been obtained from the 'true' underlying multispectral image. Note that we are assuming that the observed panchromatic and low resolution multispectral images are independent given the high resolution multispectral image we want to estimate. The Bayesian paradigm dictates that inference about the true $\mathbf{y}^b$ should be based on $p(\mathbf{y}^b|\mathbf{Y}^b, \mathbf{x}, \mathbf{y}^{\overline{b}})$ given by

$$p(\mathbf{y}^b|\mathbf{Y}^b, \mathbf{x}, \mathbf{y}^{\overline{b}}) \propto p(\mathbf{y}^b \mid \mathbf{y}^{\overline{b}}) p(\mathbf{Y}^b|\mathbf{y}^b) p(\mathbf{x}|\mathbf{y}^b, \mathbf{y}^{\overline{b}}). \tag{4}$$

Maximization of Eq. (4) with respect to $\mathbf{y}^b$ yields

$$\hat{\mathbf{y}}^b = \arg\max_{\mathbf{y}^b} p(\mathbf{y}^b|\mathbf{Y}^b, \mathbf{x}, \mathbf{y}^{\overline{b}}), \tag{5}$$

the maximum *a posteriori* (MAP) estimate of $\mathbf{y}^b$. Let us now study the degradation and prior models.

3.1 Degradation model

Given the degradation model for multispectral image super-resolution described by Eq. (1) the distribution of the observed band $\mathbf{Y}^b$ given $\mathbf{y}^b$ and $\mathbf{y}^{\bar{b}}$ is given by

$$p(\mathbf{Y}^b|\mathbf{y}^b,\mathbf{y}^{\bar{b}}) = p(\mathbf{Y}^b|\mathbf{y}^b) \propto \exp\left\{-\frac{1}{2}\beta \parallel \mathbf{Y}^b - \mathbf{H}^b\mathbf{y}^b \parallel^2\right\}. \quad (6)$$

Note that, in this formulation, $p(\mathbf{Y}^b|\mathbf{y}^b,\mathbf{y}^{\bar{b}})$ does not actually depends on $\mathbf{y}^{\bar{b}}$ since we are not considering any cross-band degradation. Using the degradation model in Eq. (3), the distribution of the panchromatic image $\mathbf{x}$ given $\mathbf{y}^b$ and $\mathbf{y}^{\bar{b}}$ is given by

$$p(\mathbf{x}|\mathbf{y}^b,\mathbf{y}^{\bar{b}}) \propto \exp\left\{-\frac{1}{2}\gamma \parallel \mathbf{x} - \lambda^b\mathbf{y}^b - \sum_{j\in\bar{b}}\lambda^j\mathbf{y}^j \parallel^2\right\}. \quad (7)$$

3.2 Image model

It is also necessary to specify $p(\mathbf{y}^b|\mathbf{y}^{\bar{b}})$, the probability distribution of the high resolution image $\mathbf{y}^b$ given the rest of the bands $\mathbf{y}^{\bar{b}}$. Although other models are possible, in this paper we assume that the prior model depends only on that band being estimated, $\mathbf{y}^b$, that is, we do not incorporate any information about the possible relations with other high resolution bands. Then, our prior knowledge about the smoothness of the object luminosity distribution within each band makes it possible to model the distribution of $\mathbf{y}^b$ by a conditional auto-regression (CAR) [8], that is,

$$p(\mathbf{y}^b|\mathbf{y}^{\bar{b}}) = p(\mathbf{y}^b) \propto \exp\left\{-\frac{1}{2}\alpha^b \parallel \mathbf{C}\mathbf{y}^b \parallel^2\right\}, \quad (8)$$

where $\mathbf{C}$ denotes the Laplacian operator, and $\alpha^{b^{-1}}$ is the variance of the Gaussian distribution.

4 Bayesian Inference

Once all the needed probability distributions are defined, the Bayesian analysis is performed. By substituting Eqs. (6), (7) and (8) into Eq. (5) we obtain

$$\begin{aligned}\hat{\mathbf{y}}^b &= \arg\max_{\mathbf{y}^b}\exp\left\{-\frac{1}{2}\alpha^b \parallel \mathbf{C}\mathbf{y}^b \parallel^2 -\frac{1}{2}\beta \parallel \mathbf{Y}^b - \mathbf{H}^b\mathbf{y}^b \parallel^2\right. \\ &\quad \left. -\frac{1}{2}\gamma \parallel \mathbf{x} - \lambda^b\mathbf{y}^b - \sum_{j\in\bar{b}}\lambda^j\mathbf{y}^j \parallel^2\right\}. \quad (9)\end{aligned}$$

(a) (b)

Figure 2. Observed Landsat 7 ETM+ image: (a) Panchromatic image; (b) From upper left to lower right, the first four bands of the multispectral image

Maximization of Eq. (9) can be carried out by an iterative gradient descendent algorithm described by

$$\mathbf{y}_{i+1}^b = \mathbf{y}_i^b - \varepsilon \left[\alpha^b \mathbf{C}^t \mathbf{C} \mathbf{y}^b - \beta^b \mathbf{H}^{b^t} (\mathbf{Y}^b - \mathbf{H}^b \mathbf{y}^b) - \gamma \lambda^b (\mathbf{x} - \lambda^b \mathbf{y}^b - \sum_{j \in \bar{b}} \lambda^j \mathbf{y}^j) \right], \quad (10)$$

where $\mathbf{y}_i^b$ and $\mathbf{y}_{i+1}^b$ are the high resolution estimates of the band b at the ith and $(i+1)$st iteration steps, respectively, and ε is the relaxation parameter that controls the convergence and the convergence rate of the algorithm.

Note that Eq. (10) also provides an iterative method to estimate the whole high resolution multispectral image. Starting with an initial estimate of the high resolution multispectral image, for each band b Eq. (10) is used to estimate the corresponding high resolution band keeping the rest of the bands fixed. After $\mathbf{y}^b$ is updated the other channels are re-estimated.

5 Experimental results

In order to test this algorithm, a Landsat 7 ETM+ image was used. The image, centered on latitude 43.178, longitude -70.933 (path 12, row 30 of the satellite) acquired on 2000-09-27, was processed at level L1G. A region of interest of the image is displayed in Figure 2. This figure depicts the panchromatic image and the first four bands of the multispectral image.

The values of λ^b in Eq. (7) can be obtained from the spectral response of the ETM+ sensor. Figure 3 depicts the (normalized to one) sensor response for each wavelength. Note that the panchromatic image covers a region of wavelengths

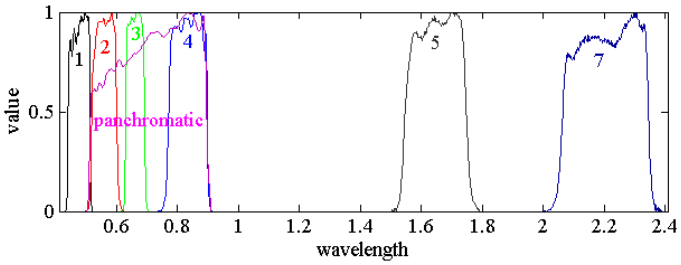

Figure 3. Landsat 7 ETM+ band spectral response.

Table 1. Obtained values for λ^b.

LANDSAT ETM+ band	λ^b	**LANDSAT ETM+ band**	λ^b
1 (0.45 μm to 0.515 μm)	0.015606	2 (0.525 μm to 0.605 μm)	0.22924
3 (0.63 μm to 0.69 μm)	0.25606	4 (0.75 μm to 0.9 μm)	0.49823
5 (1.55 μm to 1.75 μm)	0.0	7 (2.08 μm to 2.35 μm)	0.0

from almost the end of band 1 to the end of band 4, although the sensor sensibility is not constant over the whole range. By summing up the panchromatic sensor response at each multispectral image band range, and normalizing the sum to one, we obtain the values of λ^b displayed on Table 1. Note that λ^6 and λ^7 are both zero since they have no contribution to the panchromatic image.

The parameter values of the Bayesian modelling were experimentally chosen to be $\alpha^b = 1.0$, $\beta^b = 0.25$ and $\gamma^b = 0.05$, for all the bands. The gradient relaxation parameter, ε, was chosen to be equal to 1.0. Note that in order to apply Eq. (10) we also need to calculate $\sum_{j\in\overline{b}} \lambda^j \mathbf{y}^j$. Since the high resolution bands $\mathbf{y}^{\overline{b}}$ are not currently available, those bands are approximated by the cubic interpolation of the corresponding low resolution bands and the value of the sum is kept constant during the reconstruction process. The initial high resolution band $\mathbf{y}_0^b$ in Eq. (10) was obtained by cubic interpolation of its corresponding low resolution band $\mathbf{Y}^b$ and the iterative procedure was stopped when $\| \mathbf{y}_{i+1}^b - \mathbf{y}_i^b \|^2 < 0.01$.

For comparison purposes, the results obtained with the proposed method were compared with the results of cubic interpolation of the low resolution multispectral image and the Price method [7]. Figure 4 depicts bands 3 (left) and 4 (right) of the reconstructed multispectral image. This figure clearly shows that the result of the proposed method (Fig. 4(c)) is crisper than the cubic interpolated image (Fig. 4(a)) and the result of the Price method (Fig. 4(b)) while preserving the spectral characteristic of the original bands. Edges in the image are sharp and do not show the staircase effects present on the Price reconstructed image.

To better compare the results, Fig. 5 depicts the profile of the central row of the cubic interpolation of band number 4 (Fig. 5(a)) and the resulting band number 4 from the reconstruction process (Fig. 5(b)). From this profile it is clear that

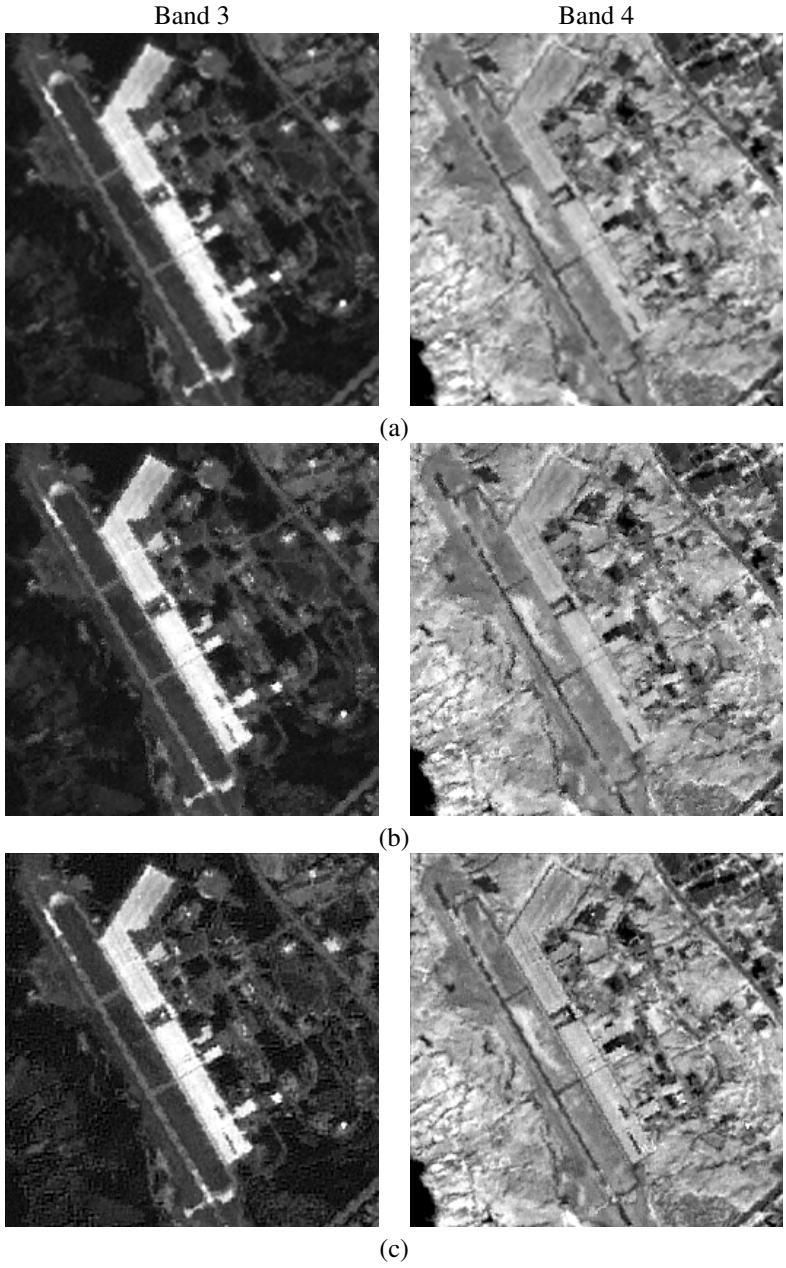

Figure 4. Reconstructed image bands 3 and 4: (a) obtained by cubic interpolation; (b) obtained by Price method [7]; (c) Obtained by the proposed method.

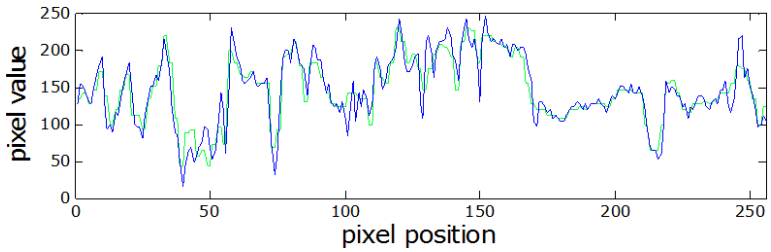

Figure 5. Central row profile for band 4 of the reconstructed multispectral image: dotted for the cubic interpolated image and solid for the reconstructed image.

both the cubic interpolated (dotted line) and the proposed method reconstruction (solid line) share the same spectral properties but the reconstructed image has a greater level of detail.

Finally, in order to validate the model in Eq. (3), the panchromatic image is compared with a simulation of the panchromatic image obtained as $\sum_{b=1}^{B} \lambda^b \hat{\mathbf{y}}^b$. Results are depicted in Fig. 6 where both the panchromatic and the reconstructed images are displayed as well as a profile of the central row of the images (Fig. 6(c)). Both images are visually indistinguishable and profiles for the panchromatic (dotted line) and reconstructed (solid line) images are almost identical, which validates the proposed model, although some high frequencies have been lost on the reconstructed image.

6 Conclusions

A new MAP method for multispectral image reconstruction has been presented. The method effectively combines the information of the panchromatic high resolution image with the low resolution multispectral image to obtain a high resolution multispectral image with the spectral characteristics of the original multispectral image and the level of detail of the panchromatic image. Preliminary results, presented on a Landsat 7 ETM+ image, validate the proposed model.

References

[1] T. Akgun, Y. Altunbasak, and R.M. Mersereau. Super-resolution reconstruction of hyperspectral images. *IEEE Transactions on Image Processing*, (in press), 2005.

[2] W. J. Carper, T. M. Lillesand, and R. W. Kiefer. The use of intensity-hue-saturation transformations for merging SPOT panchromatic and multispectral image data. *Photogrammetric Engineering and Remote Sensing*, 56(4):459–467, 1990.

[3] M.T. Eismann and R.C. Hardie. Hyperspectral resolution enhancement using high-resolution multispectral imaginary with arbitray response functions. *IEEE Transactions on Geoscience and Remote Sensing*, 43(3):455–465, 2005.

[4] P. Chavez Jr., S. Sides, and J. Anderson. Comparison of three different methods to

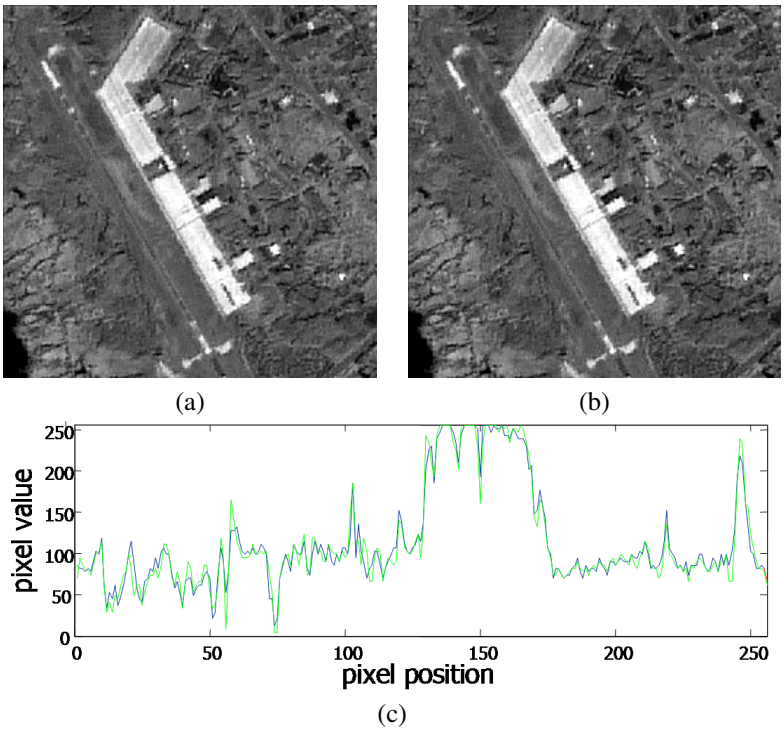

Figure 6. : (a) Panchromatic image; (b) Reconstruction of the panchromatic image from the super-resolved bands; (c) Central row profile: dotted for the panchromatic image and solid for the reconstructed image.

merge multiresolution and multispectral data: Landsat TM and SPOT panchromatic. *Photogrammetric Engineering and Remote Sensing*, 57(3):295–303, 1991.

[5] J. Nunez, X. Otazu, O. Fors, A. Prades, V. Pala, and R. Arbiol. Multiresolution-based image fusion with additive wavelet decomposition. *IEEE Transactions on Geoscience and Remote Sensing*, 37(3):1204–1211, 1999.

[6] J.H. Park and M.G. Kang. Spatially adaptive multi-resolution multispectral image fusion. *International Journal of Remote Sensing*, 25(23):5491–5508, 2004.

[7] J.C. Price. Combining multispectral data of different spatial resolution. *IEEE Transactions on Geoscience and Remote Sensing*, 37(3):1199–1203, 1999.

[8] B. D. Ripley. *Spatial Statistics*, pages 88 – 90. Wiley, 1981.

[9] V. Vijayaraj. A quantitative analysis of pansharpened images. Master's thesis, Mississippi State University, 2004.